



HAL
open science

Generation of Alveolar Epithelium Using Reconstituted Basement Membrane and hiPSC-Derived Organoids

Yong He, Elrade Rofaani, Xiaochen Huang, Boxin Huang, Feng Liang, Li Wang, Jian Shi, Juan Peng, Yong Chen

► **To cite this version:**

Yong He, Elrade Rofaani, Xiaochen Huang, Boxin Huang, Feng Liang, et al.. Generation of Alveolar Epithelium Using Reconstituted Basement Membrane and hiPSC-Derived Organoids. *Advanced Healthcare Materials*, 2022, 11 (6), pp.2101972. 10.1002/adhm.202101972 . hal-03818521

HAL Id: hal-03818521

<https://hal.science/hal-03818521>

Submitted on 18 Oct 2022

HAL is a multi-disciplinary open access archive for the deposit and dissemination of scientific research documents, whether they are published or not. The documents may come from teaching and research institutions in France or abroad, or from public or private research centers.

L'archive ouverte pluridisciplinaire **HAL**, est destinée au dépôt et à la diffusion de documents scientifiques de niveau recherche, publiés ou non, émanant des établissements d'enseignement et de recherche français ou étrangers, des laboratoires publics ou privés.

Generation of alveolar epithelium using reconstituted basement membrane and hiPSC-derived organoids

Yong He^a, Elrade Rofaani^a, Xiaochen Huang^a, Boxing Huang^a, Feng Liang^a, Li Wang^b, Jian Shi^b
Juan Peng^{a*}, and Yong Chen^{a*}

^a *École Normale Supérieure-PSL Research University, Sorbonne Universités - UPMC Univ Paris 06, CNRS UMR 8640 PASTEUR, 24, rue Lhomond, 75005 Paris, France*

^b *MesoBioTech, 231 Rue Saint-Honoré, 75001, Paris, France*

*Corresponding author. yong.chen@ens.psl.eu (Y. Chen), juan.wang@ens.psl.eu (J. Peng)

Abstract

In-vitro modelling of alveolar epithelium needs to recapitulate features of both cellular and noncellular components of the lung tissues. Herein, we present a method to generate alveolar epithelium by using human induced pluripotent stem cells (hiPSCs) and reconstituted or artificial basement membrane (ABM). The ABM was obtained by self-assembling type IV collagen and laminin with a monolayer of crosslinked gelatin nanofibers as backbone and a patterned honeycomb microframe for handling. Alveolar organoids were obtained from hiPSCs and then disassociated into single cells. After replating the alveolar cells on the ABM and a short-period incubation under submerged and air-liquid interface culture conditions, an alveolar epithelium was achieved, showing high-level expressions of both alveolar cell-specific proteins and characteristic tight junctions. Besides, endothelial cells derived from the same hiPSCs were cocultured on the backside of the epithelium, forming an air-blood barrier. Our method is generic and can potentially be applied to other types of artificial epithelium and endothelium.

1. Introduction

The human lung consists of millions of tiny sacs (alveoli) for breath and gas exchange. The inner layer of the sac is composed of squamous shape alveolar type 1 (AT1) and cuboid shape alveolar type 2 (AT2) cells and covered by a surfactant layer [1]. While about 95% of the alveolar surface is shielded by AT1 cells, the remaining part is occupied by AT2 cells which secrete the surfactant and differentiate into AT1 cells during alveolar homeostasis and post-injury repair of the alveoli. On the outer layer of the sac, blood capillaries are formed with endothelial cells (ECs), which are separated from the alveolar cells by an intermediate basement membrane. Together, AT1 and AT2 cells, intermediate BM, and ECs form air-blood barriers that are permeable to oxygen and carbon dioxide but neither to air bubbles nor to blood. Many respiratory diseases are due to damage or disorder of the alveoli, putting forward alveolar models [2,3]. The in-vitro models of alveolar epithelium are particularly attractive for both fundamental research and high throughput screening [4,5], since animal models may not be able to recapitulate all human lung features or diseases [6].

Immortalized cell lines such as A549 [7] and NCI-H441 [8] are often used in alveolar modeling but they were derived from lung tumors and may result in variable phenotypes [9]. Human-induced pluripotent stem cells (hiPSCs) [10] can now be used to generate alveolar cells with well-defined genetic or disease backgrounds [11-17]. In particular, hiPSCs can be used to produce alveolar organoids (AOs) by using different growth factors and/or inhibitors [18-20]. These AOs containing both AT1 and AT2 cells could be expanded, cryopreserved, and used for various assays. However, the ratio between AT1 to AT2 cells of the AOs remained relatively low and further processing is generally requested to reach a higher ratio. By disassociating the AOs into single cells and then replating them with a culture substrate, a higher AT1/AT2 ratio might be achievable and the resulted alveolar epithelium could be more effectively used for assessment and observation of the epithelium interface [15]. Similarly, capillary endothelial cells [21] and immune cells [22] can be derived from the same hiPSCs, providing valuable cellular resources for in-vitro modeling of air-blood barriers.

Transwell-like devices are widely used for the culture of alveolar cells and coculture of alveolar and endothelial cells [23-26]. This approach is intuitive but oversimplified, since the plastic or elastomeric membranes used in such devices are significantly different from the natural BM in terms of homogeneity and mechanic properties of the membrane. More recent studies have shown that membranes made of electrospun nanofibers or ECM hydrogels have a better biocompatibility and an improved mechanic property with respect to plastic or

elastomeric membranes [27-30]. Yet, these membranes were not thin enough or made of synthetic polymers. Knowing that the natural BM made of type IV collagen and laminin is dense thin (~100 nm thick), uniform, and highly permeable, it is important to recapitulate these essential features. Indeed, the integrity of epithelium as well as the homeostasis of the associated organ rely on these features, since the BM does not only provide a mechanical support to the epithelial cells but also precisely regulates the cell behavior through several signaling pathways [31,32]. Matrigel and other ECM hydrogels rich in type IV collagen and laminin can be used for the formation of thin films but it is difficult to reach a thickness of the order of 100 nm. Moreover, Matrigel is animal-derived containing many unknown factors so that it is not straightforward to use it for fine-tuning the cell behaviors [33]. Herein, we present a method to generate robustly alveolar epithelium by using hiPSC-derived AOs and in-vivo like BM made of ultrathin layer of type IV collagen and laminin. The in vivo like or artificial BM (ABM) was obtained by self-assembling the two BM proteins with a monolayer of crosslinked gelatin nanofibers (MNF) and a handling honeycomb microframe [34]. Without BM proteins, the MNF could be used for both hiPSC differentiation of cardiomyocytes and neurons [35,36] and primary cell culture [37-39]. After BM protein self-assembling, the MNF can be considered as backbone of the ABM. The main advantage of the ABM relies on its uniformity, low stiffness, and high permeability, in addition to its inherent bioactivity. We show that this ABM enables efficient generation of alveolar epithelium by using single cells disassociated from hiPSC-AOs and a short period of incubation under submerged and ALI culture conditions. The fabricated alveolar epithelium was analyzed by immunofluorescence microscopy and transepithelial electric resistance (TEER) monitoring [40], confirming high-level expressions of AT1 and AT2 cell-specific proteins and characteristic TEER variations. We also show that this ABM is suited for coculture of epithelial and endothelial cells derived from the same iPSCs. This method is straightforward and generic to translate hiPSC-derived organoids into engineered epithelium or endothelium that is required for modeling and high throughput studies.

2. Results

2.1 Low stiffness and high permeability of the artificial basement membrane

The ABM was designed to recapitulate the noncellular features of alveolar epithelium and to create in-vivo like alveolar tissues through AO generation and replating of dissociated AO cells (Fig. 1). The stepwise fabrication process of the ABM is depicted in Fig.S1 and the main characterization results are reported in Fig. S2. The MNF was firstly fabricated by

electrospinning with a patterned honeycomb frame and then used as backbone for self-assembling type IV-collagen and laminin [34]. A porosity of ~25% and a layer thickness of ~200 nm could be estimated for a typical MNF. After the protein self-assembling, MNF was converted to ABM with a comparable layer thickness but different bioactivity, stiffness, and permeability. A DI water contact angle of ~63° or ~38° was determined by photograph image analyses with a typical MNF membrane before and after protein self-assembling. The stiffness of the ABM could be deduced in a similar way as described in [38]. Figure S2D showed the maximum values of deflection of a 20 μm thick PDMS (polydimethylsiloxane) layer and a PDMS-ABM bilayer under pressure. By fitting the experimental data with a membrane deflection theory, the stiffness of the membranes could be deduced [38], giving an elastic modulus and a residual surface stress of $E_s = 2.2$ MPa and $\sigma_0 = 45.7$ kPa for the PDMS-ABM bilayer and $E_s = 1.3$ MPa and $\sigma_0 = 32.0$ kPa for the control (PDMS). Assuming that 1/4 deflection resistance of the bilayer is due to ABM, we then obtain $E_s = 4.9$ MPa as effective Young's modulus of the ABM. In Fig. S2E, the Darcy permeability of the MNF and the ABM are compared to that of etched in track membranes of 10 μm thickness and 0.22 μm and 0.4 μm pore sizes. These data were obtained by measuring the flow resistance of the samples as a function of pressure using a microfluidic device and automated setup [41], showing high permeability of both MNF and ABM, due to very small membrane thicknesses of the membrane and the molecular network of type IV collagen and laminin.

2.2 Generation and expansion of bud tip alveolar progenitor organoids

The hiPSC colonies were firstly generated and then subsequently converted to Definitive Endoderm, Anterior Foregut Endoderm, and Ventral-Anterior Foregut Endoderm (Fig. 1). On day 9 or 10, foregut spheroids self-aggregated, lifted away from the substrate and floated in the medium. After Matrigel droplet embedment, they were directed to bud tip progenitor organoids [42]. By culturing these progenitor cells in "CK+DCI" medium containing GSK-3 inhibitor (CHIR-99021), keratinocyte growth factor (KGF), dexamethasone, 3',5'-cyclic adenosine monophosphate (cAMP), and 3-isobutyl-1-methylxanthine (IBMX), we obtained progenitor organoids in the period of day 21 and day 42 (Fig. S3). After 2 weeks, more confluent branching structures appeared under the microscope. After 3 weeks, a rapid growing cell population which expressed NK2 homeobox 1 (NKX2.1) protein emerged, similar to that of human fetal alveolar progenitor cells [43]. These organoids could be expanded for more than 16 weeks, cryopreserved, and thawed (Fig. S4). Typically, the thawed lung bud tip organoids formed paddle-racquet-like structures and had the capacity to proliferate (Fig. S4B). To characterize

them, the progenitor organoids were dissociated into single cells and cells were replated on glass or nanofibers. A high quantity of early NKX2.1+ lung progenitors was observed (Fig. S5).

2.3 Generation and expansion of alveolar organoids

After culturing the progenitor organoids in a maturation medium, alveolar sac-like structures appeared, showing mono or multiple layers of alveoli epithelial cells. Since the maturing AOs can proliferate more rapidly, the culture medium was refreshed every 3 days and the organoids were passaged every 2 weeks. Moreover, the AOs could be also expanded, cryopreserved, and thawed, in a similar way of the bud tip progenitor organoids.

To confirm the maturation of the AOs, AT1 marker PDPN and AT2 marker SFTPC were used for immunostaining analyses, in addition to Actin marker for actin filaments. PDPN (Podoplanin) is a mucin-type transmembrane protein commonly used for AT1 cell labeling, while SFTPC (Surfactant protein C) is one of the pulmonary surfactant proteins highly expressed by AT2 cells [44]. Fig. 2 shows immunofluorescence images of small organoids formed by monolayered epithelial cells. Underneath-sections (left) and mid-sections of the organoids (right) are displayed to illustrate the distribution of the proteins. From the middle sectional view images, a well-organized actin network could be clearly seen and the cell shape and structure could be identified. More specifically, actin proteins were enriched in the apical domain of the cells toward to the single lumen, indicating a polarized organization of the cytoskeleton. The SFTPC proteins were also observed on the apical surface of cells, which could be attributed to the secretion of AT2 cells in the inner side of the cavity. In addition to the secretion in the cavity, SFTPC also expressed in the cytoplasm as shown in Fig. 2B, especially near the basal compartment. Viewed from the bottom, SFTPC protein was highly expressed on the budding front that protrudes toward the outside, showing a strong expansion ability which is the characteristic of the stem/progenitor population (Fig. 2A right). Meanwhile, less PDPN+ cells were observed and the expression of PDPN proteins were mainly in the basal domain of the cytoplasm. In terms of cell morphology, SFTPC+ cells have cuboidal shapes, with vertically elongated and relatively large nucleus (Fig. 2B, C). However, the bottom of PDPN+ cells expand to both sides to form a trapezoid shape with a flatten nucleus in the basal side. At this stage, the ratio of AT1/AT2 cells is about 2:3 (Fig. 2D). Finally, we confirmed the expression of both angiotensin-converting enzyme II (ACE2) and Transmembrane Serine Protease 2 (TMPRSS2) proteins in hiPSC-derived AOs (Fig. 2E). These two proteins are involved in SARS-CoV-2 infection, one (ACE2) serves as the binding site of the coronaviruses

and another (TMPRSS2) promotes the entry of the virus into the host cell [45]. The expression of the two proteins illustrate the maturation of the alveolar cells.

Our results show that it is feasible to generate AOs consisting of both AT1 and AT2 cells. Previous studies have shown that the hiPSC derived AOs were dominated but AT2 cells and that the AT2 cells isolated from these organoids were unable to differentiate to AT1 cells when transplanted into the bleomycin-injured lung [46]. In our case, PDPN⁺ cells were observed and tentatively attributed to AT1 and AT2 cells undergoing a phenotypic transition to AT1 cells. Nevertheless, the ratio of AT1/AT2 in AOs remains relatively low and it is interesting to develop a new method to convert AT2 into AT1 cells under ALI culture conditions.

2.4 Formation of alveolar epithelium on artificial basement membrane

After re-plating the disassociated single cells on the ABM, alveolar cells interacted with the BM proteins and self-organized to form an alveolar epithelium (Fig. 3). As it was formed by self-assembling of type-IV collagen and laminin, the ABM can be considered as two superimposed protein networks where the laminin network interacts directly with cells through integrins, dystroglycan receptors, and sulfated glycolipids [30-32]. Therefore, the ABM prompts cell adhesion and cell polarity, as well as an early setting of epithelium morphogenesis.

To control more accurately the cell number and improve the uniformity of the cell distribution on ABM, a handling device was used for cell replating on our culture device (SI method, Fig. S6). As shown in Fig. 3E, 24 h after replating cells were uniformly distributed on ABM, except for the edge effect. On the next day, cells not adhered to ABM have washed away, leaving a monolayer of tightly connected cells. Due to proliferation, the cells could reach a confluency of around 80%. For comparison, we also performed cell seeding on glass or on naked nanofibers coated with fibronectin and found that after seeding, cells aggregated to form small cysts in one day and trended to recover the 3D morphologies in 4 days (Fig. S7). Thus, the ABM is effectively conducive to cell adhesion and the early setting of epithelial monolayers. After 2 days of culture, alveolar cells were fixed and stained for SFTPC and actin filaments observation (Fig. 3D). The distribution of marked actin filaments and nuclei showed the formation of a continuous cell layer and the highly expressed SFTPC marker indicates a high population of AT2 cells. Unexpectedly, SFTPC proteins were observed mainly in the area without cells, meaning that these cell-secreted surfactant proteins can easily flow on and be captured by the monolayer of nanofibers (Fig. 3D). In addition, SFTPC expressions were also found on the cell surface (Fig. 3D, white arrows), indicating SFTPC-positive AT2 cells that account for around 10 % of the total cells of the epithelium.

2.5 Maturation of alveolar epithelium under ALI culture conditions

2.5.1 ALI culture

In order to reach a maturation stage, ALI culture was applied after submerged culture for 2 days with a membrane mounting device for a 6-well plate (Fig. 4A, Fig. S8). The period of ALI culture can vary between 3 and 7 days (Fig. 4B). Then, the cells were labeled with AT1 marker Aquaporin 5 (AQP5), AT2 marker (SFTPC), and ACE2, respectively. Here, AQP5 is a water channel protein, which plays a role in the generation of alveolar secretion [47],

In addition, the expressions of ZO-1 and E-cadherin were also examined to depict the cell junction properties. As expected, the majority of cells are AQP5+ (AT1) while more SFTPC+ (AT2) cells were detected compared with that before ALI culture (Fig. 4C-4F). Since the restrictiveness of the alveolar epithelial barrier is dependent on a series of interacting proteins comprising the adherent junctions (AJs) and tight junctions (TJs) and the core of the epithelial AJs is composed of E-cadherin which links cells to one another in the monolayer, we observed rich ZO-1+ TJs and E-Cadherin+ ATs (Fig. 4D-F). Importantly, ACE2+ cells were also observed (Fig. 4G), completing the proof of concept of alveolar epithelium formation on ABM.

2.5.2 TEER measurement

TEER measurements were firstly performed over a wide frequency range and three types of membrane, i.e., MNF, ABM, and alveolar epithelium on ABM. Our data show that in the frequency range of 10 ~ 1000 Hz, the impedance value of the ABM is higher than that of the MNF but smaller than that of the epithelium (Fig. 4G). Similar results were also obtained with other types of cells. Single frequency (12.5Hz) TEER measurements were also performed to follow the impedance variation of the derived alveolar epithelium as a function of incubation time under submerged and ALI culture conditions (Fig. 4H). Here, the impedance of the system without membrane was subtracted and all displaced values refer to that of the cell layer with the underlying ABM. Considering the fact that the epithelial cells interact directly with the ABM proteins, it would be better to the integrity and functionality of the cell-ABM system together. Clearly, the TEER values of the epithelium were all larger than that of the control (ABM) and the impedance of the epithelium increased with the incubation time. However, a significant drop of the impedance was observed the culture condition changed from submerged to ALI culture, due probably to the epithelial re-organization or loss of the established tight

junctions of the cell layer. Nevertheless, these observations are qualitatively consistent with the previous studies [40].

2.5.3 Co-culture system

An essential feature of human alveolar epithelium is the formation of an ultrathin barrier involving both alveolar basement membrane and alveolar cell layer which separates alveolar sac space and blood capillaries. A major advantage of using hiPSC lines for the development of disease-relevant models is that it allows the possibility of generating various differentiated cell types from the same cellular and genetic source, for example, endothelial cells. We have established a near-physiological manner, a coculture system of human distal lung epithelial cells and human vascular endothelial cells both derived from hiPSC, in order to study the cellular interactions of epithelium and endothelium at the alveolocapillary barrier, which could be used in both pathogenesis and recovery from an acute lung injury, and also to improve techniques of lung drug delivery. Similarly, we applied the method of dissociation and replating to get the endothelial cell layer on ABM, following the protocol of differentiation from hiPSC for vascular network organoids [21] (Fig. 5A). After 17 days, cells from matured organoids containing 30-35% endothelial cells and 60-65% pericytes [21], were prepared for seeding on nanofibers. Immunofluorescence staining identified and showed cells expressing the endothelial cell-specific CD31 marker (Fig. 5B) after replating. As shown with the result of SEM (Fig. 5C), the *in vitro* co-culture system consisting of monolayers of human alveolar epithelium obtained before and hiPSC-derived human vascular endothelial cells on the backside of the ABM, to mimic the structure of the alveolar-capillary barrier. The result showed, over the course of a three-day co-culture, two distinct cell layers grew well and did not migrate to the opposite side of the membrane (Fig. 5D, 5E). Benefiting from the ultrathin BMs only 100 nm, the two layers could strongly influence each other, containing cell morphology, cell types, and quantity.

3. Discussion

This study was based on a multiscale architecture for ABM incorporation, which compromises the robustness, flexibility, and bioactivity of the device. The objective was to prove the concept of efficient generation of human alveolar epithelium from hiPSC-derived AOs. As result, we achieved this for a period less than one week after replating the AO disassociated cells on the ABM. Our ABM device with or without cells is handleable with a tweezer, it can be placed in a culture dish or on a microscope stage, and it can be easily inserted

in a microfluidic device for organ-on-a-chip applications. Starting from this simple device configuration, sophisticated tissue organization becomes enviable [48,49].

The substrate stiffness and thickness both influence the cell behavior and tissue organization [50]. To estimate the effective stiffness of ABM, we measured the deflection of the ABM under pressure by using a microfluidic device and additional PDMS membrane. The deduced effective Young's modulus is in the order of 1 MPa, which is comparable to that of MNF and consistent with the previous studies [38], suggesting that the deflection resistance of the ABM is mainly due to that of the nanofiber backbone. In this regard, a periodic honeycomb mesh structure can be considered. Within the zeroth order approximation, the effective in-plane and out-of-plane Young modulus of the mesh should be equal to $\frac{4}{\sqrt{3}}E_s(\frac{d}{l})^3$ and $\frac{2}{\sqrt{3}}E_s(\frac{d}{l})$, respectively, where E_s is the Young's modulus of bulk material, d and l are respectively the diameter and length of the cellular segment of mesh [51]. Thus, for a mesh structure of $d/l = 0.1$, the in-plane Young's modulus should be in the kPa range, in same order of magnitude of the human lung tissue [52]. Such a stiffness match might be significant to the integrity of the alveolar epithelium [53].

At a cellular level, the influence of the substrate stiffness on cells is through focal adhesions (FAs) and actin cytoskeleton [54]. The natural BM consists of independent networks of type IV collagen and laminin, associated with cross-binding molecules such as nidogen and perlecan [30-32, 55]. The epithelial cells anchored to these networks through FAs and hemidesmosomes involving transmembrane receptors such as integrin and several signaling pathways for the regulation of cell behaviors such as adhesion, proliferation, migration, survival, and differentiation [30-32,55]. Moreover, the reconstituted BM promotes adherent junctions (AJs)-mediated cell cohesion by regulating the cytoskeleton and tension of epithelial cells. Here, FAs and AJs maintain a dynamic bio-chemical and mechanosensory crosstalk for the maintenance of epithelial architecture and homeostasis, which is requested for efficient transport of water, ions, and molecules through the transcellular and paracellular routes. We believe that the reconstituted BM enables the early setting and the long-term maintenance of the alveolar epithelium [53,56].

We would like to mention that dissociating matured organoids into single cells and then replating them on ABM allows easy assessment and observation of the epithelium interface by using such as organ-on-a-chip systems [57]. In general, organoids are multicellular systems including committed stem cells or progenitors. They can be easily expanded, cryopreserved, and thawed for downstream processing. Our results showed that the matured AOs have about

38% of PDPN+ cells and that the final alveolar epithelium has 78% of AQP5+ cells. Since the PDPN+ cells can be attributed to either AT1 cells or AT2 undergoing to AT1 cells, the resulted AQP5+ cells might be originated from these cells in addition to the proliferated and converted AT2 cells. In this regard, a longer incubation time with a lower cell seeding density might be helpful to reach a higher ratio of AT1/AT2 cells. In our experiences, we intentionally used the late stage AOs for dissociating and replating single cells on the ABM at a high cell density, in order to reach rapidly a confluent cell layer. By eliminating the extra cells above the epithelium, the remaining cells could then interact each other with the underlying BM proteins to form an epithelium in a short period.

More systematic investigations are needed to improve the quality of the alveolar epithelium and the air-blood barriers. For example, the protocols for hiPSC differentiation to blood vessel cells have to be optimized in order to produce high purity of endothelial cells. Immune cells such as alveolar macrophages and alveolar megakaryocytes derived from the same hiPSCs can be added to examine their functionality in the context of viral infection and tissue repairing. Furthermore, the fabricated alveolar epithelium can be integrated into a microfluidic device under physiological and pathological flow conditions [24]. More importantly, the impedance method has to be largely improved for in-situ monitoring over a long period (more than one week) in order to follow more closely the variation of the barrier properties with and without external stimuli. A systematic investigation is undertaken by using an automated culture system, a membrane integration device, and integrated electrodes.

4. Conclusion

We reported a method to create human alveolar epithelium by firstly generating AOs and then replating the disassociated single cells on a reconstituted BM. After a short period of incubation under submerged and ALI culture conditions, we achieved artificial alveolar epithelium with high-level expressions of AT1 and AT2 cell-specific proteins as well as characteristic tight junction proteins. The fabricated epithelium could be used for TEER monitoring and coculture with endothelial cells derived from the same hiPSCs. This study proved a strategy that can potentially be applied to other types of engineered epithelium and endothelium.

5. Experimental Section

4.1 Fabrication of ultrathin artificial basement membrane

The ultrathin ABM has been obtained by self-assembling type IV collagen and laminin in porous areas of a monolayer of crosslinked gelatin nanofibers. Briefly, photolithography and vacuum-assisted molding techniques were used to define the mold and replica of the honeycomb microframe, respectively (Fig. S1). Here, the size and thickness of the honeycomb compartments can be varied. In the present study, larger and deeper honeycomb compartments were designed for the formation of organoids while shallower ones were used for the formation of flat epithelium. The electrospinning was performed with a gelatin solution of 12 wt% gelatin powder (G2625, Sigma-Aldrich) in DI water, ethyl acetate, and acetic acid at a volume ratio of 10: 14: 21. The ejection of the gelatin solution through a needle (23-gauge) to the collector (honeycomb microframe) was controlled at a speed of 0.2 mL/h, a distance of 10 cm, a bias voltage of 11 kV, and an electrospinning time of 3 min, respectively. After deposition of the nanofibers, the sample was dried overnight in a desiccator and the gelatin nanofibers were soaked in an ethanol solution containing 2 M N-hydroxysuccinimide (NHS, Sigma-Aldrich) and 0.2 M 1-ethyl-3-(3-dimethylaminopropyl) carbodiimide hydrochloride (EDC, Sigma-Aldrich) for 4 h. The sample was finally washed three times in ethanol and dried in a vacuum chamber overnight. The as-fabricated device could be used as a substrate for cell culture. Otherwise, it could be used as a carrier or backbone for the formation of ABM. In the late case, the carrier was firstly sterilized in a 70% ethanol solution and under UV light. Then, a 50 μ L solution of laminin (20 μ g/mL, Sigma-Aldrich) and type IV collagen (1 mg/ml, Sigma-Aldrich) in DI water was dropped on. After dehydration in an incubator at 37°C for more than 4h, the deposited ECM proteins were self-assembled in the porous areas of the nanofibers to form an ultrathin membrane.

4.2 Characterization of the MNF and the ABM

The fabricated MNFs were characterized by SEM, showing high porosity and ultrathin mesh structure. By using ImageJ, a porosity of 25% was obtained. After self-assembling the BM proteins, a dense thin and flat layer was formed with the nanofiber backbone which could still be observed by SEM. A membrane thickness of ~150 nm was estimated. The stiffness of the ABM was deduced by deflection measurement in a similar way as described in [38]. Briefly, a honeycomb frame was pre-coated with viscous PDMS. A monolayer of nanofibers electrospun on a silicon wafer was then transferred to the frame. After chemical crosslinking and protein self-assembling, a 20 μ m thick PDMS layer was thermally bonded to the ABM. Before bonding the ABM device and the PDMS layer were treated by air plasma. Similarly, a sample of PDMS on honeycomb frame was prepared as control. The fabricated PDMS single

layer or PDMS-ABM bilayer (membranes) was inserted into a microfluidic device for deflection observation. DI water was injected into the upper and lower chambers separated by the membrane. A pressure was applied to the upper chamber and the deflection was observed with an optical microscopy (Zeiss Axio-Observer Z1, Germany). By searching the focal plans of the maximum and minimum deflection areas, the difference in Z was recorded as a function of applied pressure. The experimental data were then fitted in a similar way of [38], the effective Young's moduli of PDMS membrane and PDMS-ABM bilayer were determined. We also evaluated the permeability of the MNF and the ABM by measuring the flow resistance of the membranes [41]. Briefly, after integration of the MNF or ABM into a microfluidic device, the transmembrane flowrate was measured as a function of applied pressure. The flow resistance of the membrane could then be determined by using Darcy's formula and the permeability of the membrane could finally deduced considering the thickness and size of the sample.

4.3 Production of hiPSC-derived alveolar organoids

hiPSCs (episomal line, Life Technologies) were cultured in Essential 8 medium (E8, Gibco) in vitronectin (Gibco, 1:100 diluted in PBS) coated 60 mm diameter culture dish at 37 °C with 5% CO₂ [58]. Cells were passaged every 4 days at a ratio of 1:4–1:8, using 0.5 mM EDTA (Invitrogen) in DPBS (Invitrogen) for 5 min at 37 °C. The splitting ratio was adjusted in order to reach full confluency at day 4. The medium was changed daily and cells were regularly checked for mycoplasma and bacterial contamination.

AOs were produced by using the previously reported protocol [12] after minor modifications. Briefly, hiPSCs were firstly resuspended and passaged in a split ratio of 1:4 or 1:5. After culture for 24 ~ 48 h in E8, homogenous hiPSCs colonies were formed. When 60 % ~ 70 % of confluency was reached, cells were treated with definitive endoderm (DE) induction factors, 1 μM CHIR 99021 (Sigma-Aldrich) and 100 ng/mL Activin A (Stemcell Technologies) in RPMI 1640 (Gibco) supplemented with 2mM L-glutamine, 2% B27 supplement (Gibco), 1% penicillin/streptomycin (Thermo Fisher Scientific) (day 0). Cells were fed every 36–48 h by adding fresh media until day 6. For anteriorization, DE cells were treated with 1.5 μM Dorsomorphin dihydrochloride (DSM, R&D Systems) and 10 μM SB431542 (SB, R&D Systems) in a serum-free differentiation (SFD) medium containing IMDM (Gibco) supplemented with GlutaMAX, 2% B27 supplement, 1% N2 supplement (Gibco), 0.05 mg/mL L-ascorbic acid (Sigma), 1% penicillin/streptomycin from day 6 to day 10. On day 10, Matrigel and SFD medium were mixed at 1:1 volume ratio on ice. The floating foregut clumps were collected by a cut p1000 pipette tip and transferred to a 1.5-mL conical tube. Although these

clumps should settle down by gravity, they could also be gently spun down with a microcentrifuge (VWR) for ~30 s if necessary. Then, the medium was gently removed as much as possible from the tube. These foregut clumps were mixed in the Matrigel (Corning, France) solution on ice, forming a Matrigel-foregut mixture. A 24-well plate or nanofiber device was used as a substrate. Up to 25 μ L Matrigel-foregut mixture was placed on each well or nanofiber device. After gelling for 15 min ~ 30 min in an incubator, the Matrigel-foregut droplets located at the bottom of the well or on the nanofiber device were overlaid by 1 mL organoid formation medium, which is an SFD medium supplemented with 3 μ M CHIR 99021, 10 ng/mL Keratinocyte Growth Factor (KGF, Sigma-Aldrich) and 50 nM all-trans-retinoic acid (ATRA, Sigma-Aldrich). In such a way, organoids with bud tip progenitors could be derived from foregut spheroids after culture for 11 days. The expanded bud tip progenitor organoids could then be passaged every 2 weeks or placed for maturation over 3 weeks in an SFD medium supplemented with 50 nM dexamethasone (Sigma-Aldrich), 0.1 μ M 8-Br-cAMP (cAMP, Sigma-Aldrich), 0.1 μ M 3-isobutyl-1-methylxanthine (iBMX, Wako), 10 ng/ml KGF, 3 μ M CHIR 99021. During the maturation stage, the culture medium was refreshed every 3 days.

4.3 Passage, cryopreservation and thawing of alveolar organoids

The passage of either bud tip progenitor or matured AOs was performed by mechanical splitting and replating (Fig. S4A). In short, organoids were resuspended from Matrigel and broken mechanically into smaller fragments. The fragments were then resuspended in a fresh Matrigel mixture and replated to form new organoids. Due to the proliferation and differentiation of the stem cells therein, the transit-amplifying cell activities led to the continuous growth of the organoids. For both progenitors and AOs under maturation, the passage cycle is 2 weeks. More precisely, we first removed the medium from an organoid containing well with a p1000 pipette (precoated with 0.1% BSA solution for anti-sticking), and the Matrigel droplets were disrupted with 1 ml ice-cold PBS. Afterward, the organoids were collected and transferred to a 1.5 ml tube. After a gentle centrifuging in a microcentrifuge for ~30 s, PBS supernatant was removed and fresh ice-cold PBS was added, this washing step was repeated 3 times. By washing, the organoids were mechanically split into small fragments by repetitive pipetting (~100 times) with a p200 tip precoated with 0.1% BSA solution for anti-sticking. After washing, the fragments were resuspended in a 1:1 v/v Matrigel/medium solution on ice. Then, a 50 μ L (25 μ L) fragment containing a droplet was dispensed into each well of a 12 (24)-well plate. Next, the plate was reverted and incubated at 37 °C for 30 min to solidify

using a hanging-drop method [58], followed by adding 1 mL fresh organoid formation medium as mentioned above. The medium was refreshed every 3 days.

Cryopreservation with liquid nitrogen is advisable for long-term organoids storage while cryopreservation on dry ice is preferable for organoids shipment. In both cases, organoids were firstly freed from Matrigel and then resuspended in a freezing medium. Briefly, after washing and mechanically repetitive pipetting, fragments were resuspended in an organoid formation medium containing 10% DMSO and 10 μ M Y-27632 and transferred to a cryopreservation vial. Then the vial was placed in a freezing container (Mr. Frosty™), followed by moving the container into a freezer of -20°C for 10 min, into a freezer at -80°C for overnight, and finally in liquid nitrogen for long-term cryopreservation.

To thaw the cryopreserved organoids, the frozen vial was carefully defreezed and washed. The organoids were then resuspended in a 1:1 v/v Matrigel/medium solution on ice. Afterward, the organoid fragment containing solution was plated in a culture dish and incubated in a similar way as the above described.

4.4 Formation of alveolar epithelium on ABM

Maturated AOs were firstly washed by DPBS and resuspended with 1 mL Dispase (2 mg/ml) in a 15 mL conical tube placed in a 37 °C water bath for 30 min. To avoid the precipitation of the AO pellets, the Dispase solution was gently disturbed by hand agitation every 3 min. Afterward, the Dispase solution was removed as much as possible without disturbing the pellets and 2 mL TrypLE was then added into the 15 mL tube to resuspend organoids again, followed by placing it in the 37 °C water bath for 15 min. Repetitive pipetting with a p1000 tip was done every 3 min. Then, a 2 mL stop medium (IMDM + 10 % FBS) was added into the conical tube to stop the dissociation. After filtration with a 40 μ m cell strainer and centrifuging at 1000 rpm for 5 min, the cells were resuspended in a replating medium (SFD + 1.5 μ M DSM + 10 μ M SB + 50 nM Dexamethasone + 10 μ M Y-27632) at a density of 1.0×10^6 /mL. Finally, the cells were seeded on ABM at a density of 3×10^5 cells/cm² with the help of a membrane mounting device in order to reach a more homogenous cell distribution (Fig. S6). Afterward, the membrane device was placed in a 24-well plate with 1 mL fresh replating medium for submerged culture in the incubator.

After submerge-culture for cell expansion and stability during the first 2 or 3 days, the membrane was mounted in a homemade ALI culture device for the maturation of the epithelial layer. The device was placed in a 6-well plate in which the basolateral space was immediately

filled with 1.3 mL ALI culture medium (maturation medium with 5% FBS) and the medium in the apical side, if any, was removed to ensure a good ALI culture.

4.5 Co-culture of hiPSC-derived epithelial and endothelial cells

HiPSC-derived vascular endothelial cells were obtained using the differentiation protocol of [21]. An agarose-coated nanofiber device was used as a low-attachment substrate for the formation of spherical embryoid bodies. After cell seeding and incubation for 24 h (Day 0), the hiPSC culture medium was replaced by a mixture of DMEM/F12 medium and neurobasal medium, supplemented by B27-vitamin A, N2, and Glutamax. Meanwhile, 12 μ M CHIR99021 and 30 ng/ml BMP4 were added to orient the hiPSCs to the mesoderm direction for 3 days. Then, the supplementary molecules were replaced by 100 ng/ml VEGFA and 2 μ M dcAMP for the vascular lineage differentiation for 2 days. On day 5, the vascular endothelial progenitor spheroids on nanofibers were wrapped with a mixed solution of Geltrex and collagen I for gel layer formation at 37°C. Then, the assembly was merged in a Stempro-34 nutrient medium, supplemented with 2mM L-Glutamine, 100 ng/ml VEGFA, and 100 ng/ml bFGF for the vascular network maturation. After maturation for 5 days, the vascular cells were checked by immunostaining microscopy with CD31 biomarker. After another 6 days, the formed vascular networks were dissociated and the resulted endothelial cells were replated on the backside of the alveolar epithelial for co-culture using the same dissociation and replating protocols as above described.

4.6 Immunofluorescence staining and imaging

AOs were fixed using 4% paraformaldehyde in PBS for 30 min and rinsed with PBS three times. The fixed cells were permeabilized with 0.5% Triton X-100 in PBS for 30 min at room temperature and then incubated in a blocking solution containing 3% v/v bovine serum albumin, 0.1% Triton X-100 and 0.1% v/v Tween 20 in PBS overnight to block out non-specific bindings. The cells were stained with primary antibodies at 4°C for overnight and then incubated with fluorescent second antibodies at room temperature for 2 h. Next, samples were incubated in a PBS buffer solution containing 4'-6-diamidino-2-phenylindole (DAPI, Invitrogen, 1:100) and actin (ActinRed™ 555, Invitrogen) for nuclear and actin staining respectively, during another 30 min at room temperature. Finally, cells were washed with PBS three times, each time for 15 min. The coverslips were mounted using Prolong Gold (Invitrogen). The stained organoids were observed with confocal microscopy (Zeiss, LSM710) and the images were collected as TIF files and analyzed with software ImageJ.

The primary antibody ZO-1 (1:100), E-cadherin (1:100), SFTPC, (1: 25), CD31 (1:50), NKX2.1, ACE2 (1:1000) and TMPRSS2 (1:100) were from Invitrogen. PDPN (1: 50) and AQP5 (1: 80) were from Santa Cruz Biotechnology. All Alexa Fluor conjugated secondary antibodies are from Invitrogen, and all the corresponding secondary antibodies were diluted in 1:250.

4.7 Scanning Electron Microscope (SEM)

Co-cultured alveolar epithelium and endothelium were observed by SEM (Hitachi TM 3000) operated at 10 kV. Cell samples were fixed in PBS containing 4% formaldehyde for 30 min, then they were washed twice with PBS and immersed in 30% ethanol for 30 min. Afterward, cell samples were dehydrated in graded series of ethanol with increasing concentrations of 50%, 70%, 80%, 90%, 95%, 100%, respectively, and each for 10 min. After drying with a nitrogen gas flow, a 5 nm-thick gold layer was sputtered on the samples prior to the SEM observation.

4.8 Transepithelial Electrical Resistance (TEER) measurement

The integrity of the alveolar epithelium can be monitored by measuring TEER of the cell layer. Conventionally, the TEER measurements are performed with a Boyden chamber in which a permeable filter insert is used to support the cell culture and to separate the chamber into apical (or upper) and basolateral (or lower) compartments [39]. Two electrodes, one placed on the apical side and the other on the basolateral side, are used for either direct current (DC) or alternating current (AC) measurement. In this work, a Millicell-ERS system (Millipore Corp., Bedford, USA) was used which is based on the AC measurement with a fixed frequency (12.5 Hz) and “chopstick” electrodes. In addition, a Discovery 2 system (Analog Devices, Wilmington, USA) was adopted, together with a customized Python script, for the impedance spectroscopy measurements over a broad frequency range.

The measurement process includes measuring the blank resistance of ABM without cells (R_{blank}) and the resistance of ABM with cells (R_{total}). The resistance of the cell layer (R_{cell}) can then be calculated as $R_{cell} = R_{total} - R_{blank}$. In our case, the ABM-supported epithelium was mounted in an ALI culture device (Fig. S8) in which the basolateral side was filled with 2 mL and the apical side filled with 200 μ L replating medium. Before TEER measurements, the electrodes were sterilized by merging them into 70% ethanol for 15 min and equilibrated by soaking them in PBS and IMDM medium subsequently. The culture media were replaced by a fresh IMDM medium (5 mL in the basolateral side and 600 μ L on the apical side). Data were

then recorded five times for each measurement. After the measurement, the IMDM medium was replaced again by the replating and maturation media to maintain the cell culture.

4.9 Statistical analysis

All group data are expressed as mean \pm SEM. The comparisons between groups were performed using Student t-test. Differences between groups were considered significant when $P < 0.05$ (* $P < 0.05$; ** $P < 0.01$; *** $P < 0.001$).

Acknowledgements

The authors thanks Prof. Armelle Baeza-Squiban and Dr. Jean-françois Berret from the Université de Paris for fruitful discussions. This work has received support from French National Research Agency (ANR-17-CE09-0017, ANR-10-IDEX-0001-02 PSL, and ANR-10-LABX-31), Région Ile-de-France (DIM-ELICIT), PSL-valorization (program pre-maturation), Carnot-IPGG, and European Commission Cost Action (BIONECA, CA 16122).

References:

- [1] L. Knudsen, M. Ochs *Histochemistry and Cell Biology*. **2018**, *150*, 661.
- [2] J. A. Whitsett, T. E. Weaver *Am J Respir Cell Mol Biol*. **2015**, *53*, 1.
- [3] K. V. Evans, J.-H. Lee *STEM CELLS Translational Medicine*. **2020**, *9*, 867.
- [4] M. Nikolic, T. Sustersic, N. Filipovic *Frontiers in bioengineering and biotechnology*. **2018**, *6*, 120.
- [5] H. Viola, K. Washington, C. Selva, J. Grunwell, R. Tirouvanziam, S. Takayama *Adv Healthc Mater*. **2021**, *10*, 2100879.
- [6] F. Barré-Sinoussi, X. Montagutelli *Future Sci OA*. **2015**, *1*, FSO63.
- [7] K. A. Foster, C. G. Oster, M. M. Mayer, M. L. Avery, K. L. Audus *Exp Cell Res*. **1998**, *243*, 359.
- [8] A. F. Gazdar, B. Gao, J. D. Minna *Lung Cancer*. **2010**, *68*, 309.
- [9] J. J. Salomon, V. E. Muchitsch, J. C. Gausterer, E. Schwagerus, H. Huwer, N. Daum, C. M. Lehr, C. Ehrhardt *Mol Pharm*. **2014**, *11*, 995.
- [10] K. Takahashi, K. Tanabe, M. Ohnuki, M. Narita, T. Ichisaka, K. Tomoda, S. Yamanaka *Cell*. **2007**, *131*, 861.
- [11] S. X. Huang, M. D. Green, A. T. de Carvalho, M. Mumau, Y. W. Chen, S. L. D'Souza, H. W. Snoeck *Nat Protoc*. **2015**, *10*, 413.
- [12] A. Jacob, M. Morley, F. Hawkins, K. B. McCauley, J. C. Jean, H. Heins, C. L. Na, T. E. Weaver, M. Vedaie, K. Hurley, A. Hinds, S. J. Russo, S. Kook, W. Zacharias, M. Ochs, K. Traber, L. J. Quinton, A. Crane, B. R. Davis, F. V. White, J. Wambach, J. A. Whitsett, F. S. Cole, E. E. Morrissey, S. H. Guttentag, M. F. Beers, D. N. Kotton *Cell Stem Cell* **2017**, *21*, 472.
- [13] Y. Yamamoto, S. Gotoh, Y. Korogi, M. Seki, S. Konishi, S. Ikeo, N. Sone, T. Nagasaki, H. Matsumoto, S. Muro, I. Ito, T. Hirai, T. Kohno, Y. Suzuki, M. Mishima *Nature Methods*. **2017**, *14*, 1097.
- [14] L. Tamò, Y. Hibaoui, S. Kallol, M. P. Alves, C. Albrecht, K. E. Hostettler, A. Feki, J. S. Rougier, H. Abriel, L. Knudsen, A. Gazdhar, T. Geiser *Am J Physiol Lung Cell Mol Physiol*. **2018**, *315*, L921.
- [15] K. M. Abo, L. Ma, T. Matte, J. Huang, K. D. Alysandratos, R. B. Werder, A. Mithal, M. L. Beermann, J. Lindstrom-Vautrin, G. Mostoslavsky, L. Ikonomidou, D. N. Kotton, F. Hawkins, A. Wilson, C. Villacorta-Martin, bioRxiv [Preprint]. 2020 Jun 4:2020.06.03.132639. doi: 10.1101/2020.06.03.132639.
- [16] J. R. Lorsch, F. S. Collins, J. Lippincott-Schwartz *Science*. **2014**, *346*, 1452.
- [17] C. Pan, C. Kumar, S. Bohl, U. Klingmueller, M. Mann *Mol Cell Proteomics*. **2009**, *8*, 443.

- [18] Y. W. Chen, S. X. Huang, A. L. R. T. de Carvalho, S.-H. Ho, M. N. Islam, S. Volpi, L. D. Notarangelo, M. Ciancanelli, J. L. Casanova, J. Bhattacharya, A. F. Liang, L. M. Palermo, M. Porotto, A. Moscona, H. W. Snoeck *Nature Cell Biology*. **2017**, *19*, 542.
- [19] E. Magro-Lopez, C. Palmer, J. Manso, I. Liste, A. Zambrano *Stem Cell Research & Therapy*. **2018**, *9*, 186.
- [20] A. J. Miller, B. R. Dye, D. Ferrer-Torres, D. R. Hill, A. W. Overeem, L. D. Shea, J. R. Spence *Nature Protocols*. **2019**, *14*, 518.
- [21] R. A. Wimmer, A. Leopoldi, M. Aichinger, D. Kerjaschki, J. M. Penninger *Nature Protocols*. **2019**, *14*, 3082.
- [22] D. Bernareggi, S. Pouyanfard, D. S. Kaufman *Experimental hematology*. **2019**, *71*, 13.
- [23] S. van Riet, D. K. Ninaber, H. M. M. Mikkers, T. D. Tetley, C. R. Jost, A. A. Mulder, T. Pasman, D. Baptista, A. A. Poot, R. Truckenmüller, C. L. Mummery, C. Freund, R. J. Rottier, P. S. Hiemstra *Scientific Reports*. **2020**, *10*, 5499.
- [24] D. Huh, B. D. Matthews, A. Mammoto, M. Montoya-Zavala, H. Y. Hsin, D. E. Ingber *Science*. **2010**, *328*, 1662.
- [25] A. O. Stucki, J. D. Stucki, S. R. R. Hall, M. Felder, Y. Mermoud, R. A. Schmid, T. Geiser, O. T. Guenat *Lab on a Chip*. **2015**, *15*, 1302.
- [26] T. Bluhmki, S. Traub, A.-K. Müller, S. Bitzer, E. Schruf, M.-T. Bammert, M. Leist, F. Gantner, J. P. Garnett, R. Heilker *Scientific Reports*. **2021**, *11*, 17028.
- [27] P. Zamprogno, S. Wüthrich, S. Achenbach, G. Thoma, J. D. Stucki, N. Hobi, N. Schneider-Daum, C.M. Lehr, H. Huwer, T. Geiser, R. A. Schmid & O. T. Guenat, *Commun Biol*. **2021**, *4*, 168.
- [28] N. Higueta-Castro, M. T. Nelson, V. Shukla, P. A. Agudelo-Garcia, W. Zhang, S. M. Duarte-Sanmiguel, J. A. Englert, J. J. Lannutti, D. J. Hansford & S. N. Ghadiali, *Sci Rep*, **2017**, *7*, 11623
- [29] E. Dohle E, S. Singh, A. Nishigushi, T. Fischer, M. Messling, M. Möller, R. Sader, J. Kasper, S. Ghanaati, C.J. Kirkpatrick, *Tissue Eng Part C Methods*. **2018**, *24*, 495.
- [30] M. Radiom, Y. He, J. Peng-Wang, A. Baeza-Squiban, J.-F. Berret, Y. Chen *Biotechnology and Bioengineering*. **2020**, *117*, 2827.
- [31] M. Paulsson *Crit Rev Biochem Mol Biol*. **1992**, *27*, 93.
- [32] P. D. Yurchenco *Cold Spring Harb Perspect Biol*. **2011**, *3*, 1.
- [33] C. S. Hughes, L. M. Postovit, G. A. Lajoie *Proteomics*. **2010**, *10*, 1886.
- [34] E. Rofaani, J. Peng, L. Wang, Y. He, B. Huang, Y. Chen *Microelectronic Engineering* **2020**, *232*, 111407.

- [35] Y. Tang, L. Liu, J. Li, L. Yu, L. Wang, J. Shi, Y. Chen *Nanoscale*. **2016**, *8*, 14530.
- [36] Y. Tang, L. Liu, J. Li, L. Yu, F. P. U. Severino, L. Wang, J. Shi, X. Tu, V. Torre, Y. Chen *Journal of Materials Chemistry B*. **2016**, *4*, 3305.
- [37] Y. Tang, F. P. Ulloa Severino, F. Iseppon, V. Torre, Y. Chen *Microelectronic Engineering*. **2017**, *175*, 61.
- [38] M. Radiom, Y. He, J. Peng-Wang, A. Baeza-Squiban, J.F. Berret, Y. Chen, *Biotechnol. Bioeng*. **2020**, *117*, 2827.
- [39] G. Pitingolo, Y. He, B. Huang, L. Wang, J. Shi, Y. Chen *Microelectronic Engineering*. **2020**, *231*, 111371.
- [40] B. Srinivasan, A. R. Kolli, M. B. Esch, H. E. Abaci, M. L. Shuler, J. J. Hickman *Journal of Laboratory Automation*. **2015**, *20*, 107.
- [41] F. Liang et al, to be published
- [42] R. F. Conway, T. Frum, A. S. Conchola, J. R. Spence *BioEssays*. **2020**, *42*, 2000006.
- [43] A. J. Miller, D. R. Hill, M. S. Nagy, Y. Aoki, B. R. Dye, A. M. Chin, S. Huang, F. Zhu, E. S. White, V. Lama, J. R. Spence *Stem Cell Reports*. **2018**, *10*, 101.
- [44] K. H. Wu, N. Tang, *Development* **2021**, *148*, dev193458
- [45] S.L. Leibel, and S. Xin, *The EMBO Journal*, **2021**, *40*, e107651.
- [46] R. Jayadev, D. R. Sherwood *Curr Biol*. **2017**, *27*, R850.
- [47] P. Flodby, C. Li, Y. Liu, Y. *Sci Rep* 2017, *7*, 3473 (2017).
- [48] J. C. Rose, L. De Laporte *Adv Healthc Mater*. **2018**, *7*, e1701067.
- [49] M. Viola, S. Piluso, J. Groll, T. Vermonden, J. Malda, M. Castilho *Adv Healthc Mater*. **2021**, 2101021.
- [50]. Mullen CA, Vaughan TJ, Billiar KL, McNamara LM. *Biophys J*. 2015;108(7):1604
- [51] L. J. Gibson, M. F. Ashby, *Cellular Solids: Structure and Properties*, Cambridge University Press, Cambridge **1997**.
- [52] C. F. Guimarães, L. Gasperini, A. P. Marques, R. L. Reis *Nature Reviews Materials*. **2020**, *5*, 351.
- [53] L. R. Smith, S. Cho, D. E. Discher *Physiology (Bethesda)*. **2018**, *33*, 16.
- [54] J. L. Eisenberg, A. Safi, X. Wei, H. D. Espinosa, G. S. Budinger, D. Takawira, S. B. Hopkinson, J. C. Jones *Res Rep Biol*. **2011**, *2*, 1.
- [55] R. Jayadev, D. R. Sherwood *Curr Biol*. **2017**, *27*, R207.
- [56] L. Zhao, M. Yee, M. A. O'Reilly *Am J Physiol Lung Cell Mol Physiol*. **2013**, *305*, L409.
- [57] A. Geraili, P. Jafari, M. S. Hassani, B. H. Araghi, M. H. Mohammadi, A. M. Ghafari, S. H. Tamrin, H. P. Modarres, A. R. Kolahchi, S. Ahadian, A. Sanati-Nezhad *Adv Healthc Mater*.

2018, 7, 1700426.

[58] M. Panek, M. Grabacka, M. Pierzchalska *Cytotechnology*. **2018**, 70, 1085

Figure caption

Figure 1 Process overview of hiPSC differentiation toward alveolar epithelium. (A) Schematic of the process from hiPSC to alveolar organoids, single-cell replating on artificial basement membrane (ABM), and air-liquid interface (ALI) culture. (B) Protocol and timeline of the process. DSM/SB: Dorsomorphin dihydrochloride/SB431542; D: Dexamethasone; Y: Y-27632 rock inhibitor; CK: CHIR 99021 + KGF; DCI: Dexamethasone +cAMP+ IBMX; FBS: fetal bovine serum. (C) Bright-field images of hiPSCs (day 0), hiPSC derived definite endoderm (day 6), emerged anterior foregut endoderm (day 9), bud tip progenitor organoids in Matrigel (day 39), and alveolar epithelium on ABM (day 45).

Figure 2 Confirmation of alveolar cell phenotype in matured alveolar organoids. (A) Immunofluorescent underneath-sections (left) and mid-sections of the organoids (right) showing markers of AT1 cells (Podoplanin, PDPN) and AT2 cells (surfactant protein C, SFTPC). Actin filaments were stained to show the shape and structure of the cell. The white stars indicate the luminal cavities. Scale bar, 50 μ m. (B) Zoom images of the white boxes in (A). (C) Intensity plot along the white dotted lines in B. (D) Percentage of the AT1 and AT2 cell numbers. (E) Immunofluorescence images after ACE2 (green) and TMPRSS2 (red) labeling.

Figure 3 Replating of organoid dissociated single cells. (A) Schematic of the process. (B) Photograph of a monolayer of nanofiber (MNF) and handing device for cell seeding placed in a 6-well culture plate. (C) Bright-field images of replated cells on an MNF, showing the cell layer in a honeycomb compartment of the device before and after removing the unattached cells. (D) Immunofluorescence images of the cells after submerged and ALI culture for 2 and 3 days. Cells were stained with SFTPC (green) and Actin (red). Cross-section images are also shown below. (E) Radial plot (ImageJ) of SFTPC signals a honeycomb compartment. From the center to the edge, the compartment was divided into two parts of equal sizes (center and periphery). (F) Bar graph of the SFTPC intensity in the center and periphery areas.

Figure 4 Characterization of alveolar epithelium on an artificial basement membrane. (A) Photograph of an ABM handing device for ALI culture placed in a 6-well plate. (B) Bright field images of replated cells on ABM after culture for 2 (submerge) or 5 (submerged + ALI) days. (C-E) Immunofluorescence images of the cells after submerged and ALI culture for 5 days. AT1 and AT2 cells were labeled with AQP5 and SFTPC antibodies, respectively. Tight junctions were labeled with ZO-1 antibody, adheres junctions were labeled with E-cadherin

antibody. ACE2 proteins expressed in cells were also stained. (F) Percentage of the SFTPC or AQP5 positive cells. (G) Impedance spectra of three types of samples. (H) Absolute resistance of the epithelium under submerged and ALI culture conditions.

Figure 5 Co-cultivated alveolar epithelium and endothelial cells. (A) Differentiation protocol of hiPSCs to vascular cells. (B) Immunofluorescence images of replated vascular cells labelled with CD31. (C) SEM images of co-cultured alveolar epithelium on one side and endothelium on the other side of ABM. (D) Left: Schematic of ALI co-culture of ABM supported alveolar epithelium (upper) and endothelium (lower). Right: Cross-sectional view of co-cultured alveolar epithelium and endothelium. (E) Immunofluorescence images showing alveolar and endothelial cells. Actin filaments were stained to show two different cell organizations.

Figure 1

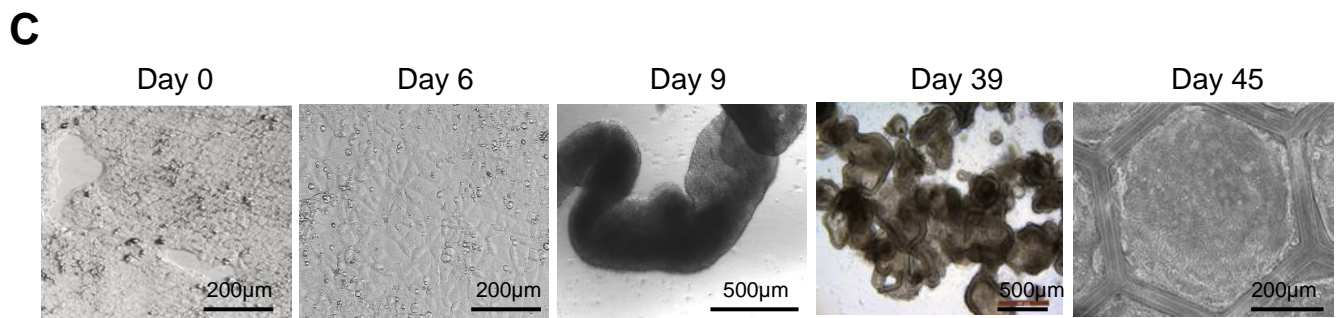
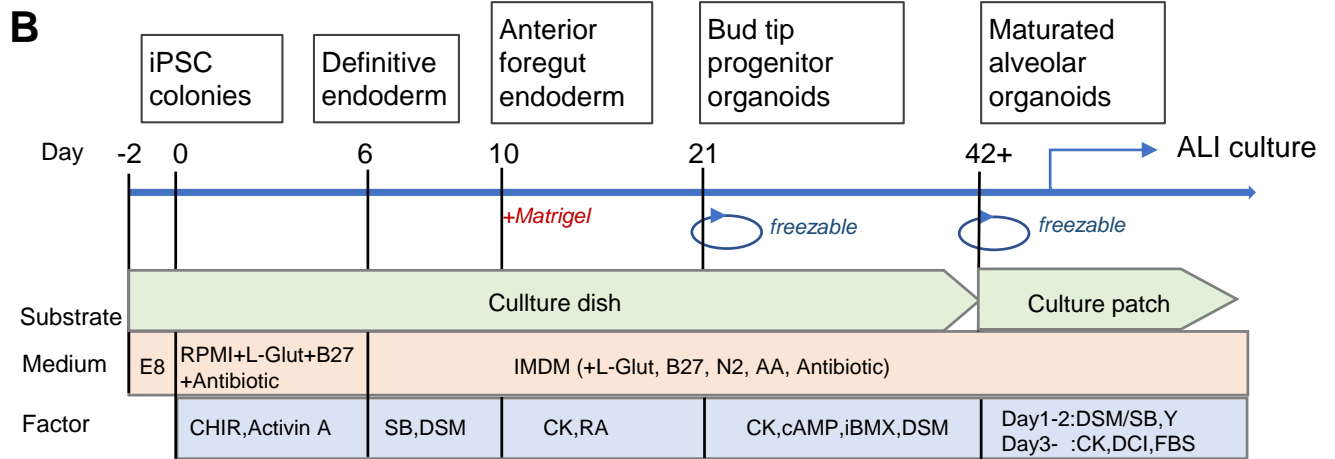
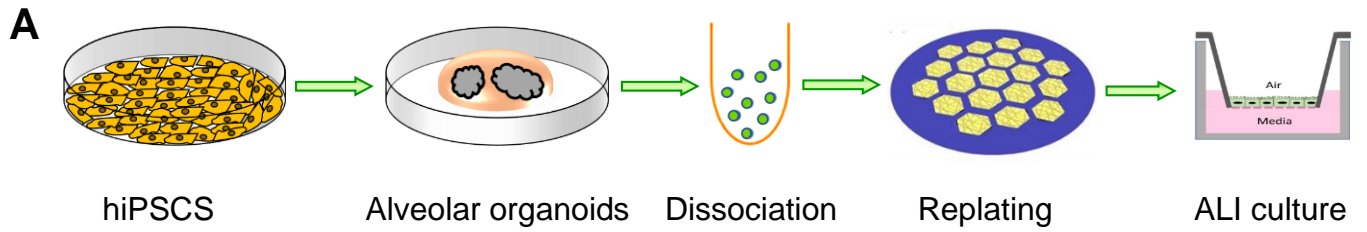
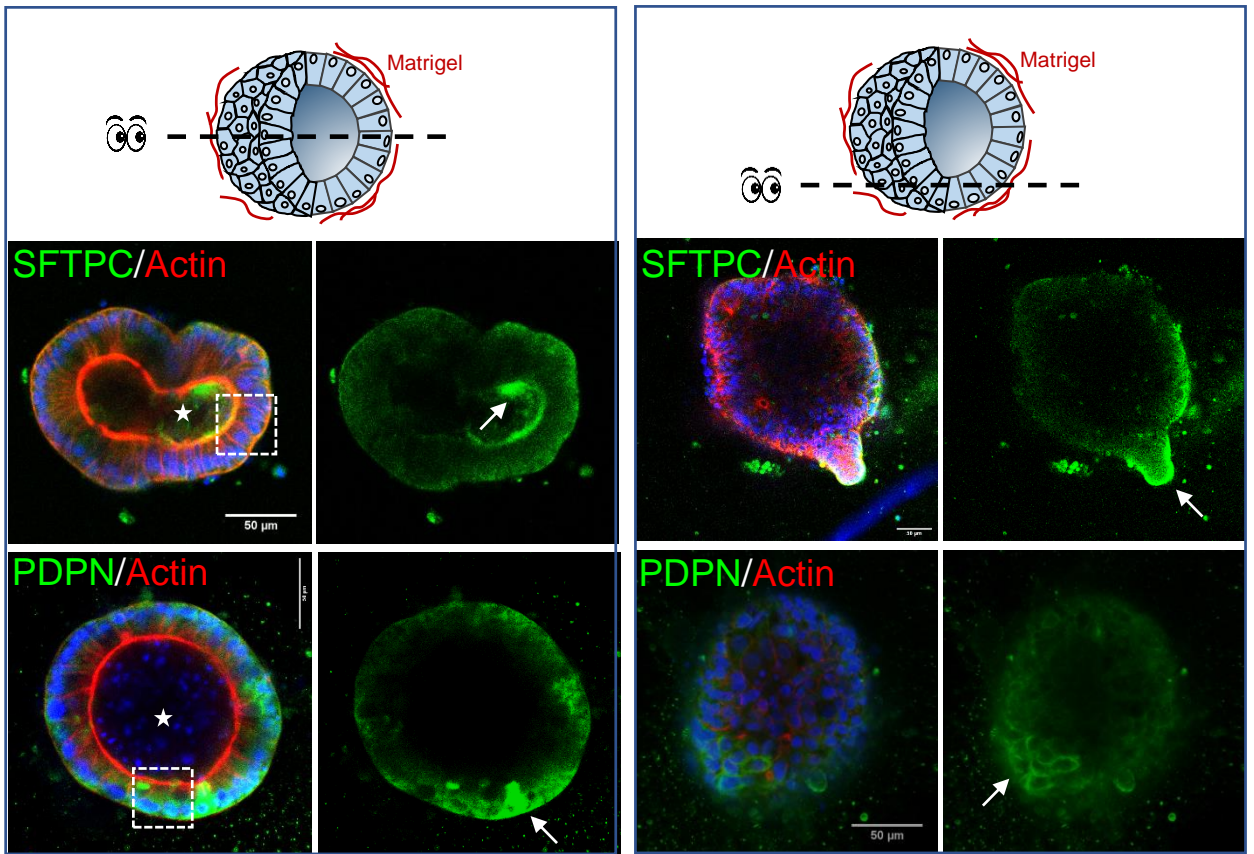
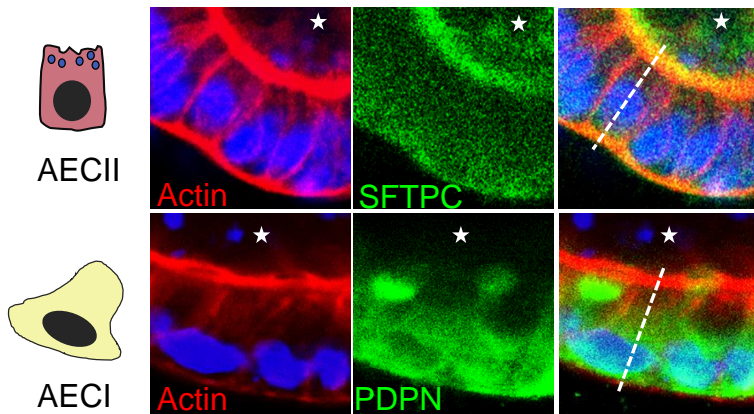


Figure 2

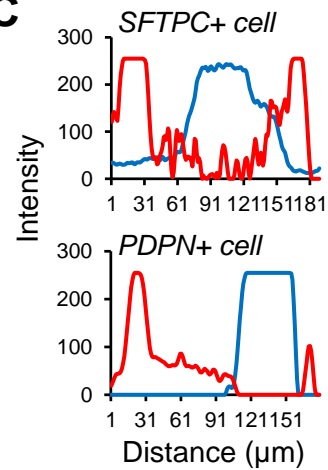
A



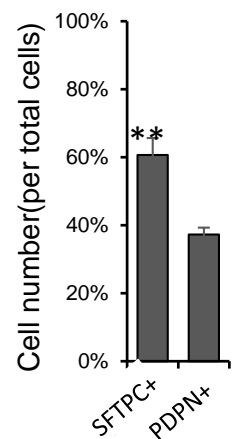
B



C



D



E

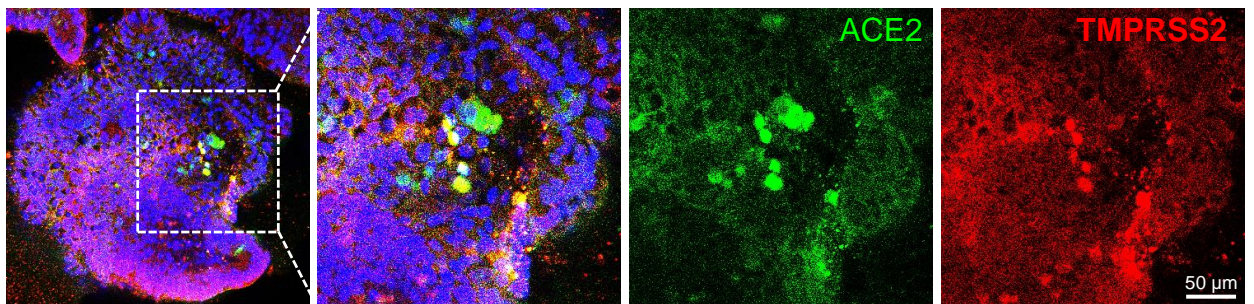


Figure 3

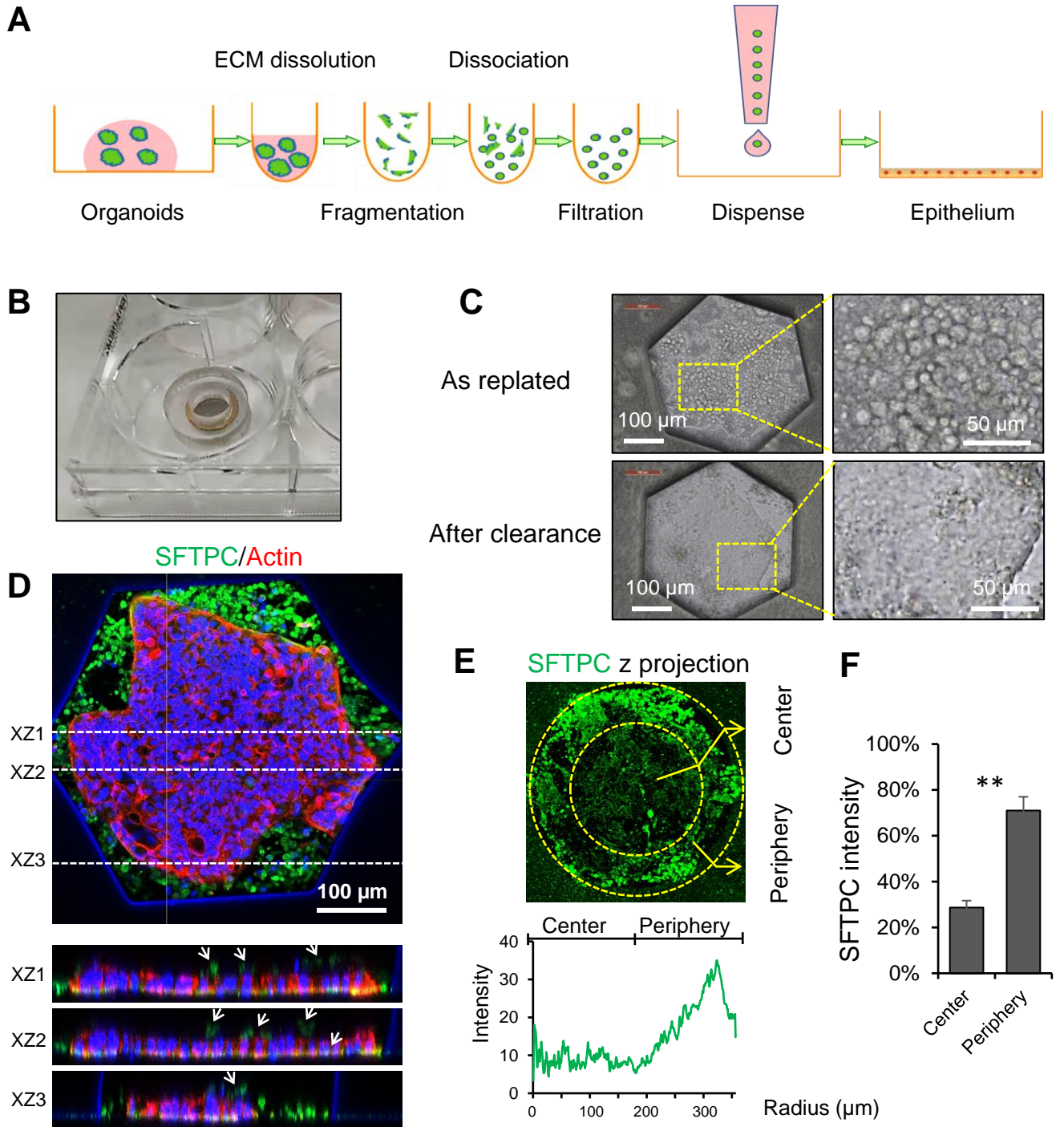


Figure 4

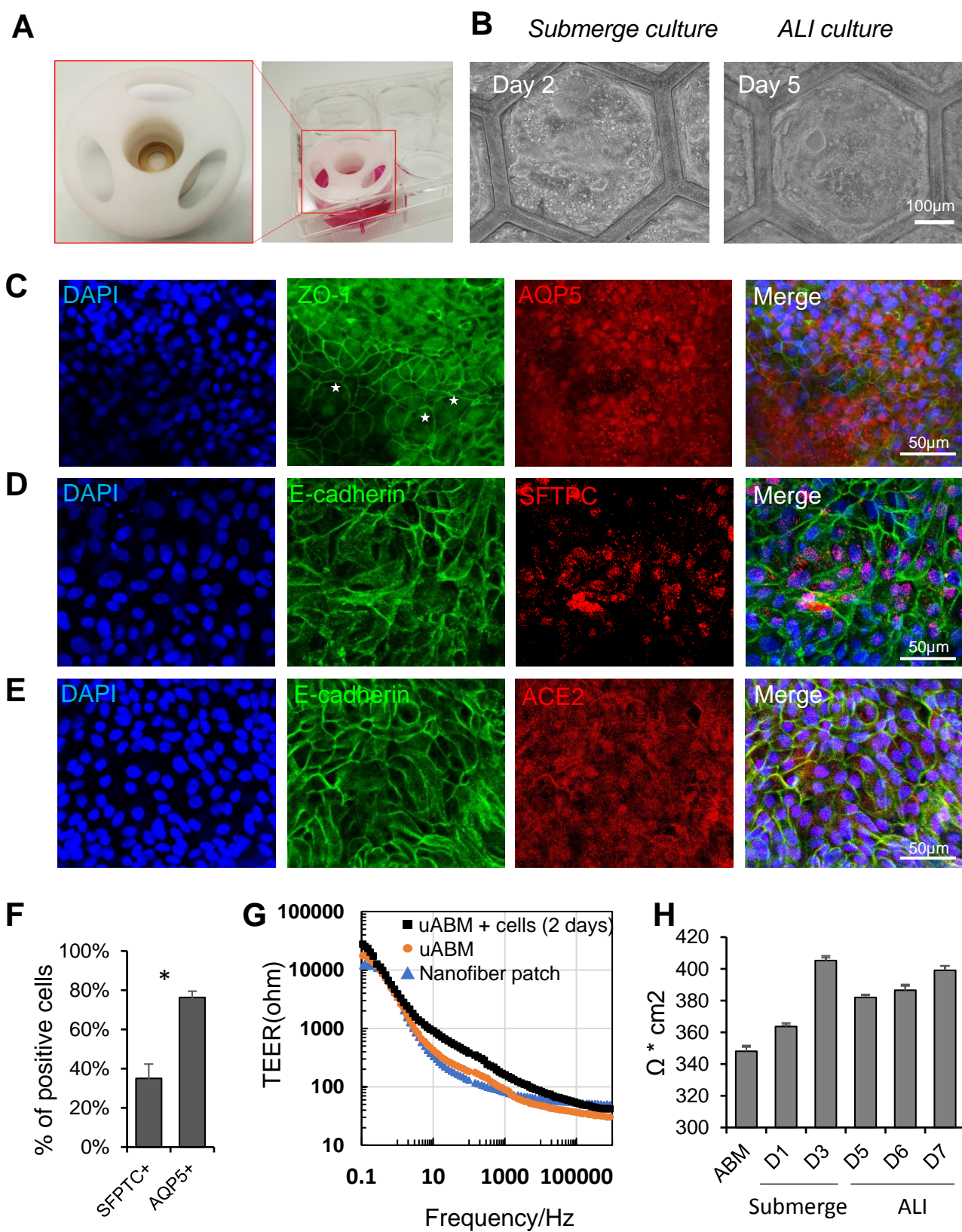
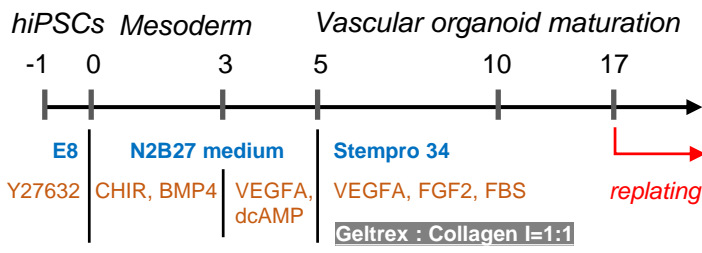
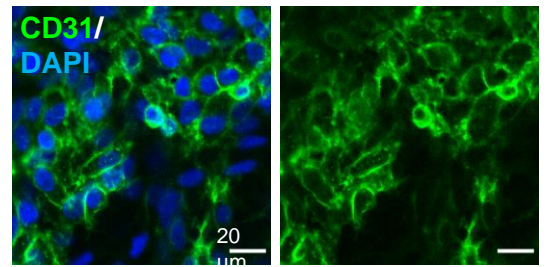


Figure 5

A

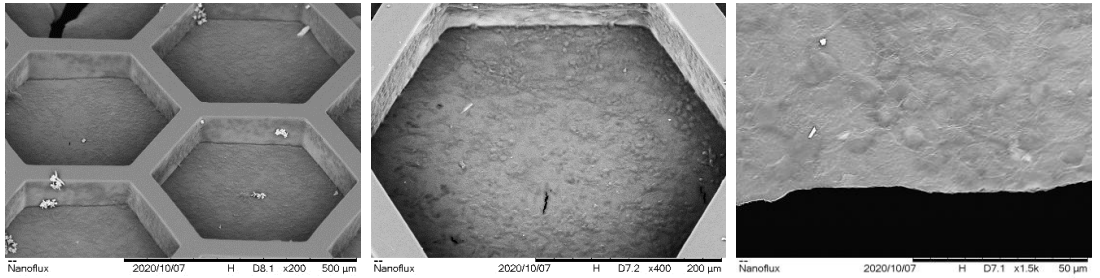


B

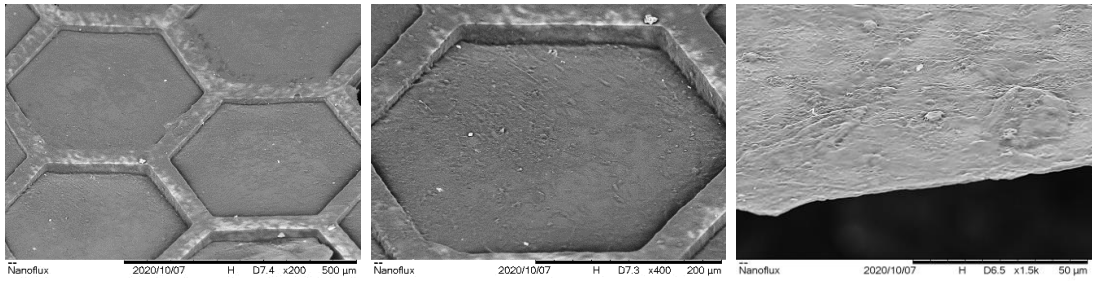


C

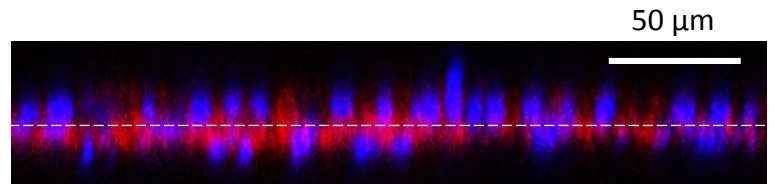
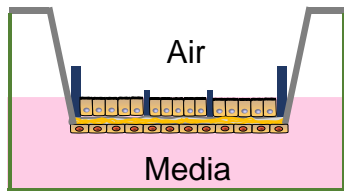
Alveolar epithelium



Capillary endothelium

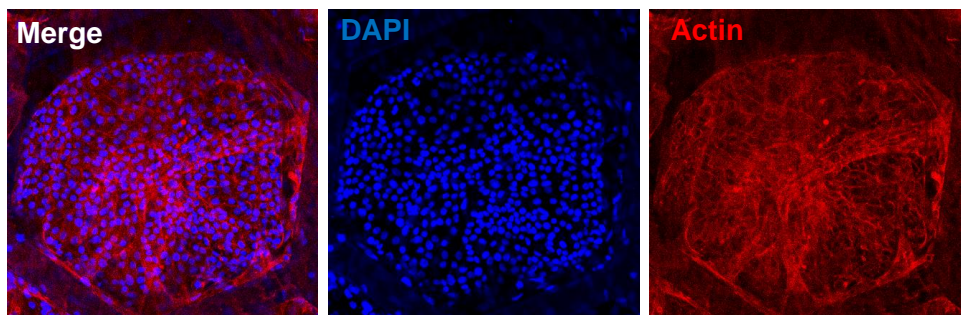


D



E

Alveolar epithelium



Capillary endothelium

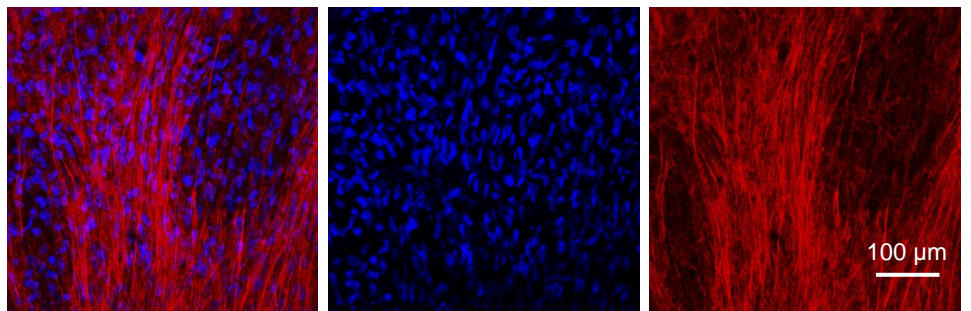


Figure S1

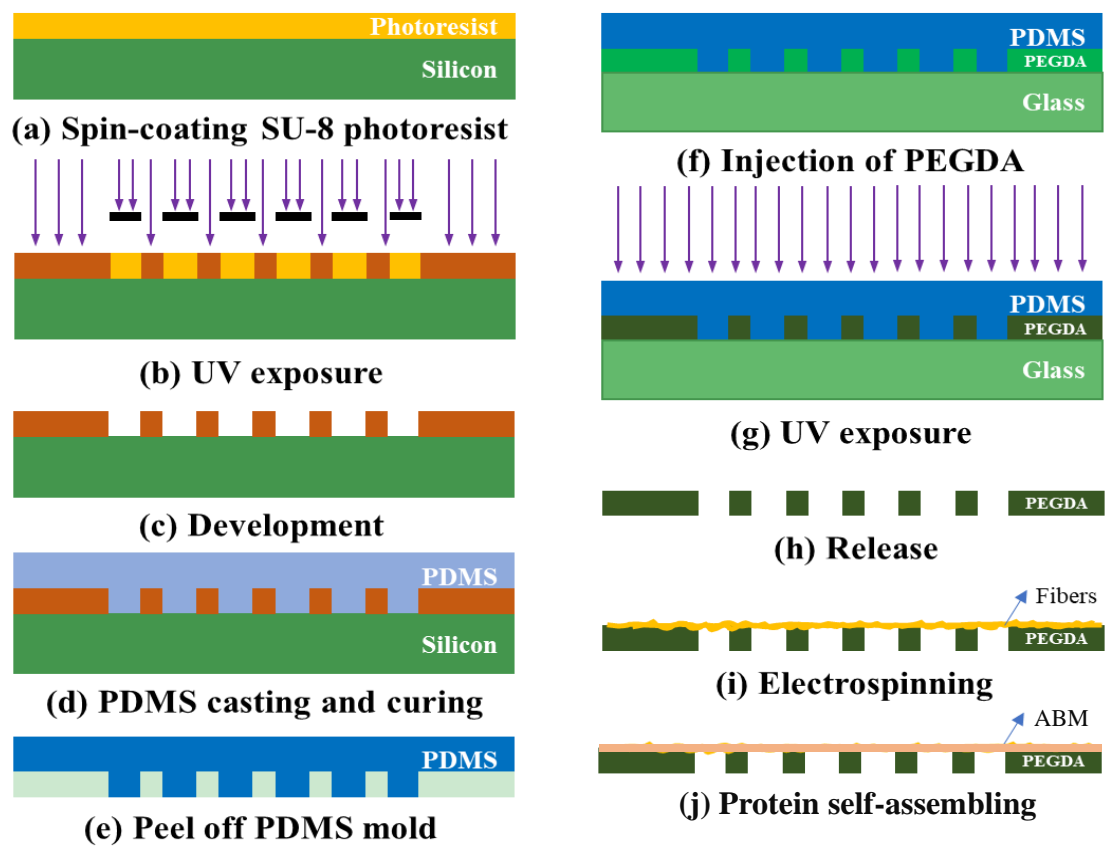


Figure S2

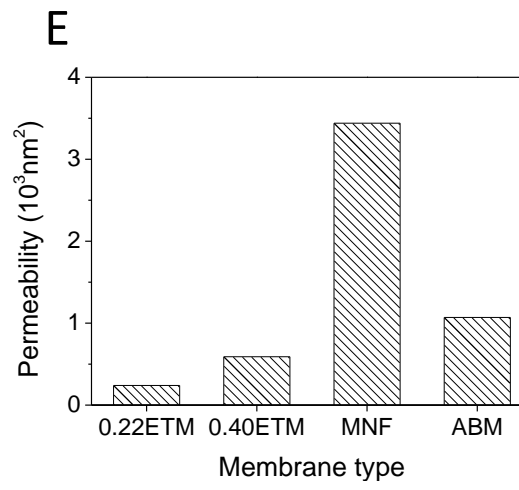
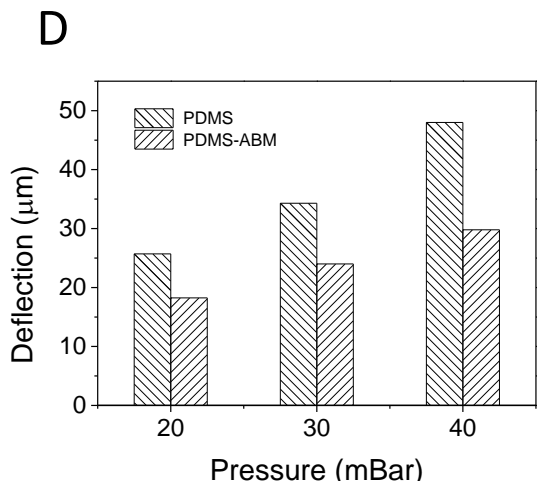
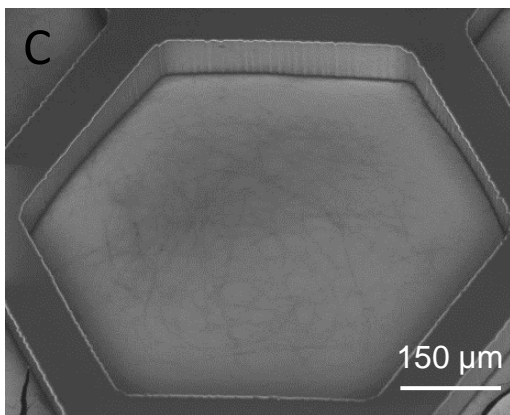
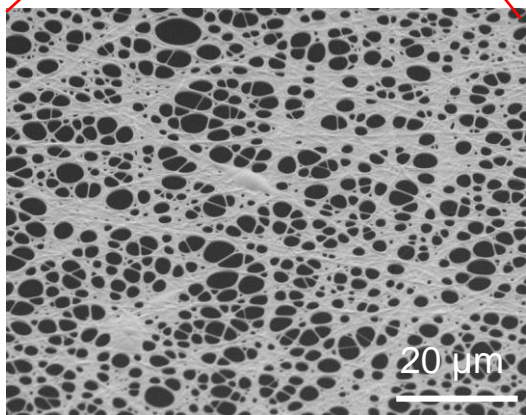
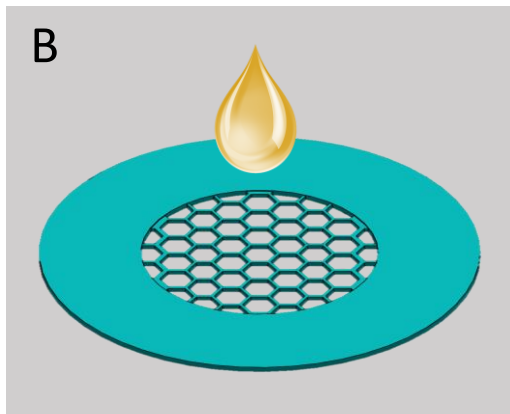
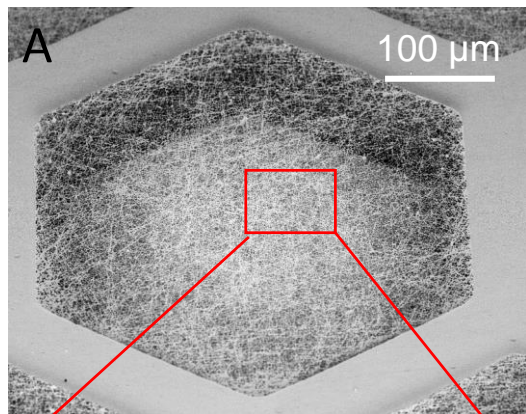


Figure S3

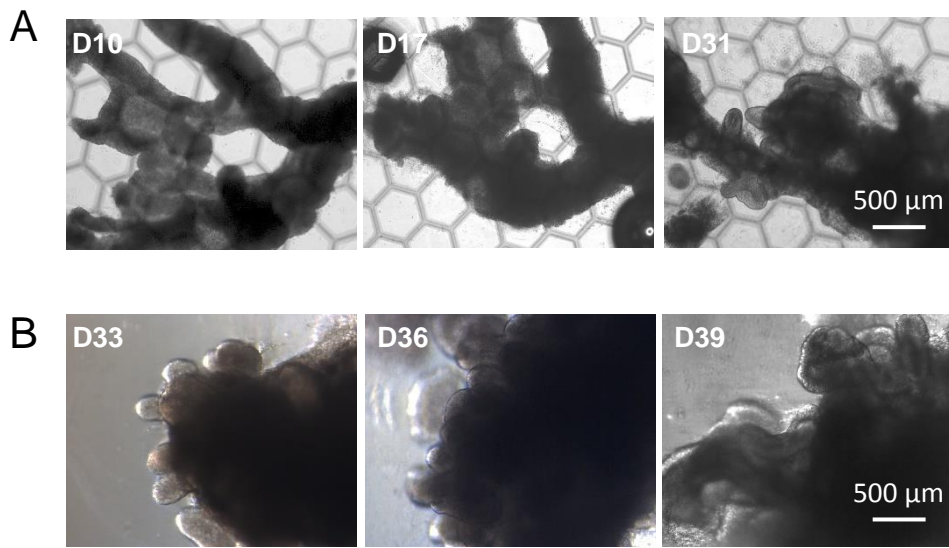


Figure S4

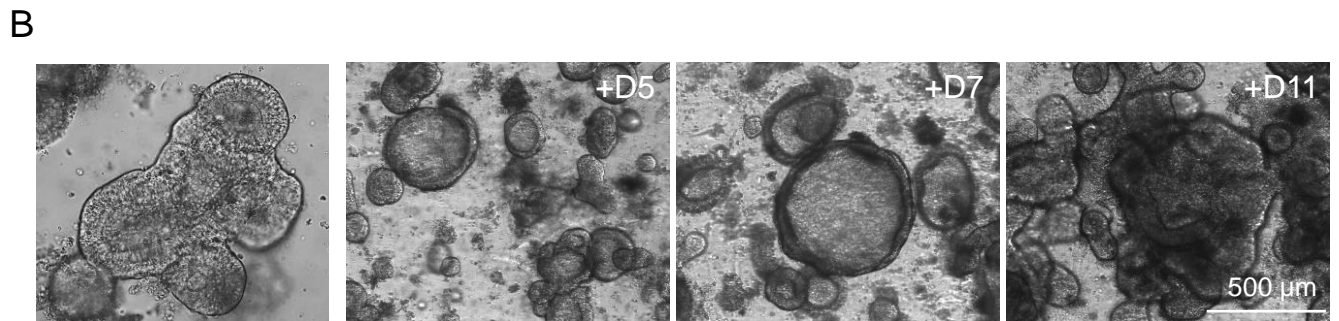
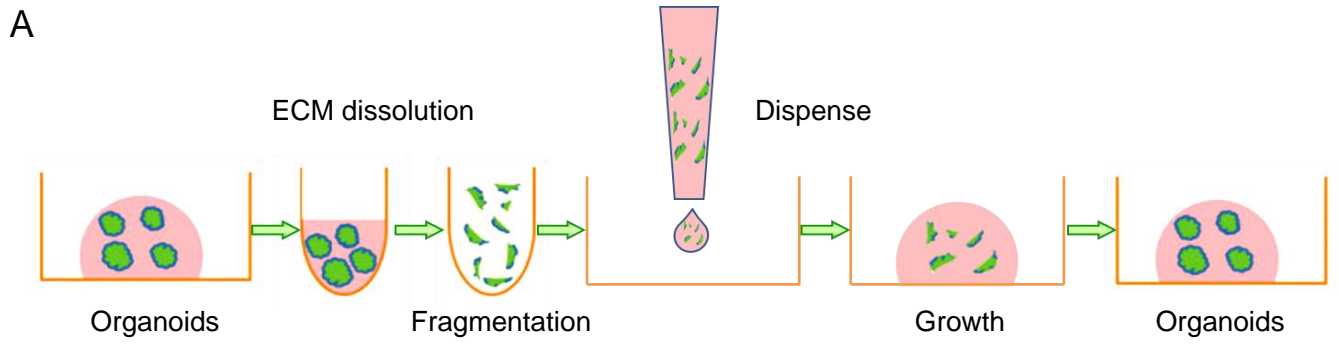


Figure S5

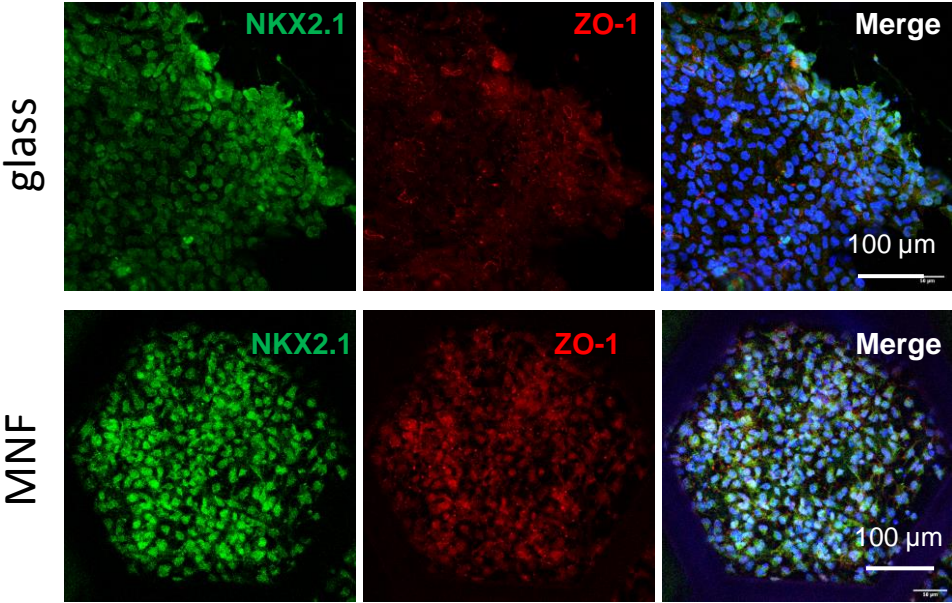


Figure S6

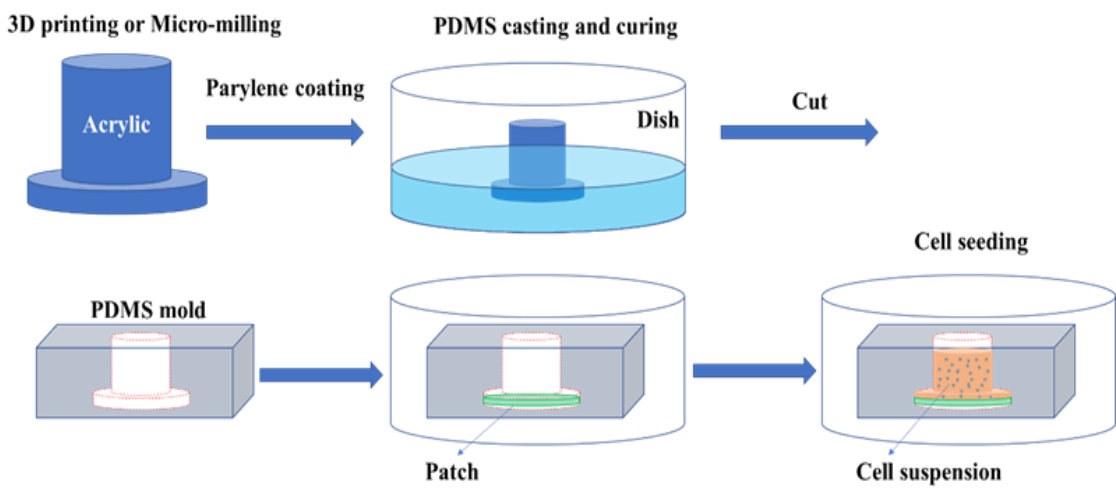


Figure S7

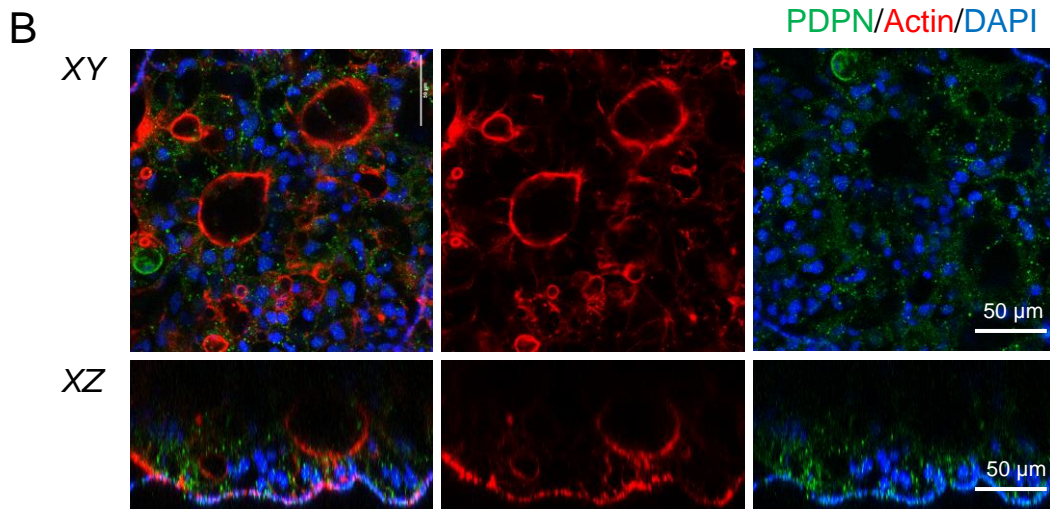
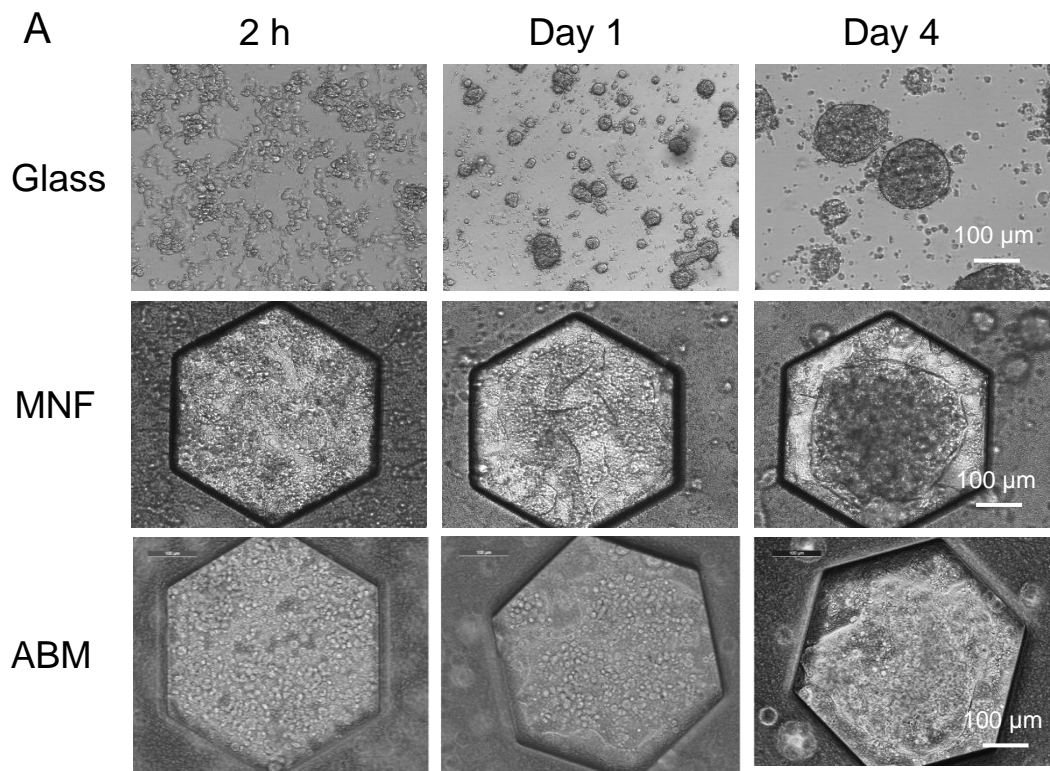


Figure S8

